Long-Term Coastal Upwelling over a Continental Shelf–Slope

NOBUO SUGINOHARA AND YOSHITERU KITAMURA

Geophysical Institute, Faculty of Science, University of Tokyo, Bunkyo-ku, Tokyo, 113 Japan

(Manuscript received 13 December 1983, in final form 19 March 1984)

ABSTRACT

Long-term coastal upwelling over a continental shelf–slope with emphasis on the planetary dispersion of Rossby waves is studied with numerical models. The ocean is forced by a wind stress with a limited longshore extent. The thermocline intersects the shelf–slope and the internal radius of deformation is smaller than the width of the shelf–slope. Two case studies with and without the β effect are studied. The early-stage response within a week or so is similar between the two. For an f-plane case, the whole-stage response is accounted for by coastal-trapped wave dynamics, and only equatorward flow exists over the shelf–slope at an advanced stage. However, inclusion of the β effect leads to a significant change in the alongshore flow pattern at the advanced stage. Due to the westward Rossby dispersion of the equatorward flow associated with the first and second coastal-trapped mode responses, the poleward undercurrent develops in the thermocline layer over the shelf. The time for the undercurrent to appear depends on the speed of the westward dispersion of the second-mode response. The undercurrent obtained in the present model may represent the one observed off Oregon and California.

1. Introduction

For an understanding of coastal upwelling circulation, effects of a continental shelf–slope are essential. The reason is that in the typical coastal upwelling regions such as those off California and Oregon, the internal radius of deformation is smaller than the width of the shelf–slope, and coastal-trapped waves, which can be identified neither as internal Kelvin nor as barotropic shelf waves (Huthnance, 1978), play a fundamental role in determining the upwelling circulation. The forerunner to this paper (Suginohara, 1982, hereafter referred to as I) studied coastal upwelling over a continental shelf–slope on an f-plane induced by a wind stress with a limited longshore extent, and demonstrated the role played by the coastal-trapped waves emanating from the southern edge of the forcing region (a short review is given in Section 3). Marked differences in upwelling circulation from that for a flat bottom ocean (Yoon and Philander, 1982) were well recognized, although only short-term upwelling events starting with an ocean at rest were studied.

Off Oregon, favorable winds for upwelling continue to blow throughout the upwelling season with fluctuations both in speed and direction; off California, the favorable winds persist throughout the year. Direct current measurements have revealed evolution of the equatorward coastal jet and the poleward undercurrent associated with coastal upwelling. Huyer *et al.* (1975) pointed out that off Oregon the poleward undercurrent over the shelf exists as a mean alongshore flow only in late summer, i.e., near the end of the upwelling season. Recent observations off California show that the poleward undercurrent at mid-depth over the mid-shelf persists at least from spring through summer (Allen, personal communication, 1983). A poleward undercurrent was reproduced in I, but it was only a transient feature and existed over the deeper part of the shelf–slope.

There is a need to study the coastal upwelling caused by long-time persisting winds. It is expected that with an increase in the time scale, the latitudinal gradient of the Coriolis parameter, the β effect, plays an important role. McCreary (1981) and Philander and Yoon (1982) studied long-term coastal upwelling for a flat bottom ocean and documented the westward dispersion of the alongshore flow by the β effect. In an inviscid model, the equilibrium state in the wake of the westward Rossby dispersion is a state of no motion with the meridional pressure gradient in exact balance with the wind stress with no curl. But in the presence of dissipation, there are steady currents such as the equatorward coastal jet and the poleward undercurrent in the final equilibrium state. McCreary (1981) and Philander and Yoon (1982) indicated that their results for a flat bottom ocean have many features in common with observations at eastern boundaries, especially the coastal jet and the poleward undercurrent.

In these flat bottom models, the formation of the coastal jet and the poleward undercurrent is due to the Kelvin-wave mode response of many vertical modes; the higher modes are selectively dissipated by vertical dissipation, whereas the lower modes are dispersed westward as Rossby waves. However, as pointed

out in I, only coastal-trapped waves, which are neither internal Kelvin nor barotropic shelf waves, exist in a typical situation of density stratification and bottom topography for coastal upwelling regions such as off Oregon and California. Thus, the different mode structures, which yield the different coastal response characteristics, may lead to significant changes in Rossby wave dispersion and dissipation.

The purpose of the present study, as the direct extension of I, is to describe long-term coastal upwelling over a continental shelf–slope. Two case studies are discussed and contrasted. In the first, as the reference experiment, an f-plane model is studied. The evolution of the upwelling circulation may be explained by coastal-trapped wave dynamics alone. Next, to conclude the present paper, the effect of the Rossby dispersion over the shelf–slope is studied with a β-plane model.

2. Model

We consider a stratified ocean adjacent to a meridional eastern boundary in the Northern Hemisphere. The ocean is also bounded by artificial northern, southern and western boundaries. A schematic view of the model ocean is shown in Fig. 1. The latitudinal width of the ocean is 1830 km and the longitudinal width is 2880 km. It has a continental shelf–slope of 112 km width, uniform in the longshore direction, and the depth is 1570 m. Governing equations are the same as used in I. We also follow the boundary conditions of I except the heat exchange through the sea surface, i.e., at the sea surface the density flux,

$$\frac{\gamma}{\rho_0 C_v}(\rho^* - \rho)$$

is imposed, where C_v is the specific heat at constant volume, ρ the surface layer density, and $\rho^* = 24.0$ (in σ_t units) is the initial value for the surface layer density. The coefficient of the heat flux γ is taken to be 100 cal (°C cm^2 day)$^{-1}$. Only a southward wind stress uniform in the east–west direction with a limited longshore extent is considered (Fig. 2). The wind stress increases gradually to its steady state value within three days.

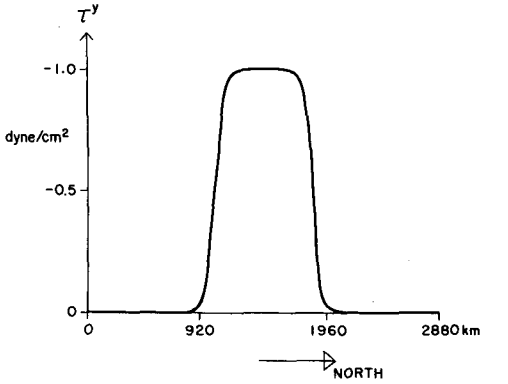

FIG. 2. Longshore distribution of the equatorward wind stress.

At the initial state the ocean is at rest, and the density stratification is horizontally uniform. The initial stratification with the configuration of the continental shelf–slope is shown in Fig. 3. The main thermocline intersects the shelf–slope and the seasonal thermocline is taken into account. This may represent a typical situation for Oregon and California.

The numerical method used in the present experiment is that of I. As shown in Fig. 3, there are sixteen levels in the vertical direction. In the upper 220 m, a regular spacing of 20 m is taken. There are 71 × 73 horizontal grid points. In the north–south direction,

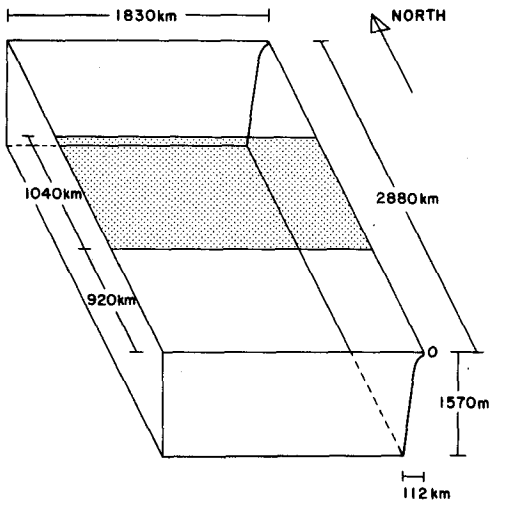

FIG. 1. Schematic view of the model ocean. Shaded zone indicates the forcing region.

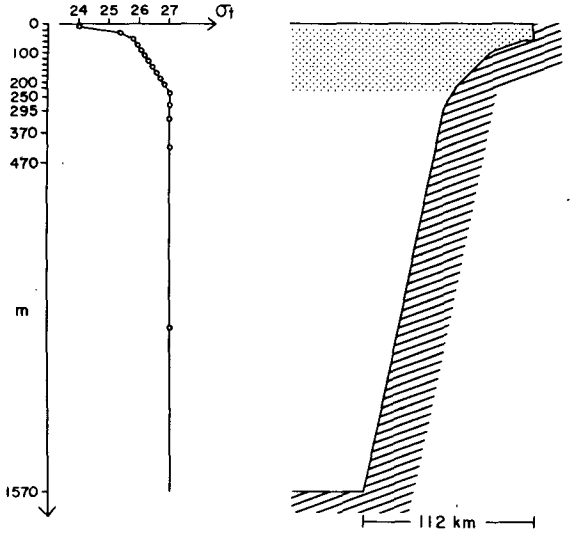

FIG. 3. Initial density stratification and configuration of the shelf–slope.

the grid interval is 40 km. In the east–west direction, the grid points are irregularly spaced. Resolution is highest near the eastern boundary where the grid interval is 4 km for a distance of 128 km from the coast. The spacing then increases gradually until it reaches a maximum value of 267 km.

The following values are used for numerical calculations: the coefficient of the vertical eddy viscosity is 10 $cm^2\ s^{-1}$; the horizontal eddy viscosity, 6×10^6 $cm^2\ s^{-1}$; the coefficient of the vertical eddy diffusion, 0.1 $cm^2\ s^{-1}$; and the horizontal eddy diffusion is 10^3 $cm^2\ s^{-1}$. To avoid smoothing out the initial density stratification, the coefficients of diffusion are taken as small as possible. With heating through the sea surface, this yields a well-mixed layer that is always confined to the top layer; i.e., a layer 20 m thick. The western and southern boundaries are treated artificially. Near these boundaries, a Newtonian damping term is included and the coefficient of lateral friction is increased by a factor of 100 compared with the interior value in order to create a very dissipative region. These regions work quite well to prevent disturbances generated along the western boundary (downwelling) from propagating to the eastern side of the basin.

3. Results

a. The f-plane case

The Coriolis parameter is taken to be $5 \times 10^{-5}\ s^{-1}$ and is constant over the whole domain. The radius of deformation for the gravest baroclinic mode defined in the offshore flat bottom area is ~24 km, a distance smaller than the width of the shelf–slope. Sequential patterns of the alongshore flow, onshore–offshore circulation and density along the zonal section at the center of the forcing region are shown in Figs. 4a, b and c. In Figs. 5a, b and c the time evolution of the streamfunction and alongshore flow along the coast are also plotted.

The early-stage response to the onset of the winds has been studied in detail in I and is as follows (refer to I). Initially, Ekman offshore flow and compensating onshore flow are induced, and equatorward flow develops over the shelf–slope. Then, coastal-trapped waves generated at the southern edge of the forcing region begin to affect the upwelling circulation. When the first-mode wave arrives (around day 5 at this section), the onshore compensating flow offshore of the coastal area begins to decrease in strength, and eventually offshore flow accompanied by downwelling dominates. Thus, the upwelling tends to be confined to the coastal area. The equatorward flow also tends to be confined to the coastal area, and the poleward undercurrent commences to develop below the main thermocline over the shelf–slope. When the second-mode wave arrives (around day 17 at this section), the upwelling region tends to be further confined to the coastal area, and the coastal jet and poleward undercurrent stop accelerating.

Next we discuss the evolution at an advanced stage. After the second-mode wave passes, the coastal jet gradually approaches its steady state, and the poleward undercurrent decreases in strength and finally disappears. Eventually, only equatorward flow exists over the shelf–slope. The equatorward flow tends to extend farther offshore. This extension is a feature associated with the advection of the upwelled water by Ekman transport (see Fig. 4c). For the onshore–offshore circulation there is no remarkable change either in pattern or strength. Thus, the drastic changes in upwelling circulation occur only in association with the passage of the first and second mode waves.

For the density section (Fig. 4c) associated with the early-stage response, the isopycnals over the shelf–slope considerably upslope toward the coast, and reach the sea surface. Then, the upwelled water tends to be carried offshore by the Ekman transport. At the advanced stage, the offshore advection of the upwelled water is suppressed by the effect of the heating. The isopycnals in the lower part of the main thermocline bend downward toward the slope, which reflects the dominance of downwelling over the deeper part of the shelf–slope and also indicates a marked vertical shear of the alongshore flow.

A rather strong offshore flow is found in the upper part of the offshore area of Fig. 4b. This flow is the motion associated with an anticyclonic vortex induced by the effect of the marked displacements of the thermocline, a frontal structure, as was studied by Suginohara (1977). This vortex keeps growing as long as the forcing continues (Fig. 5a); the evolution of the streamfunctioin field (total transport field) is shown in the figure. With the arrival of the first-mode wave, the streamfunction field ceases to develop. Hence, the equatorward coastal jet is accompanied by a marked total transport over the shelf. Then, the offshore transport in the forcing region tends to increase gradually in strength, though variations occur with the passage of the second-mode wave (see Fig. 5a).

The dynamics of the evolution may be explained as follows: Each of the coastal-trapped wave mode responses can be divided into a locally forced response and a remote response associated with a wave generated at the southern edge of the forcing region. The locally forced response is two-dimensional in that it is independent of the alongshore coordinate. The forced alongshore flow is accelerated steadily, but the forced onshore–offshore circulation attains its steady state soon after the onset of the winds. With passage of the mode wave, an alongshore pressure gradient for each mode is established to balance the wind stress, yielding a steady state for this mode response. When the first-mode wave arrives, the upwelling tends to be confined to the coastal area, and the coastal jet is formed. The rest of the modes keep evolving, and the poleward

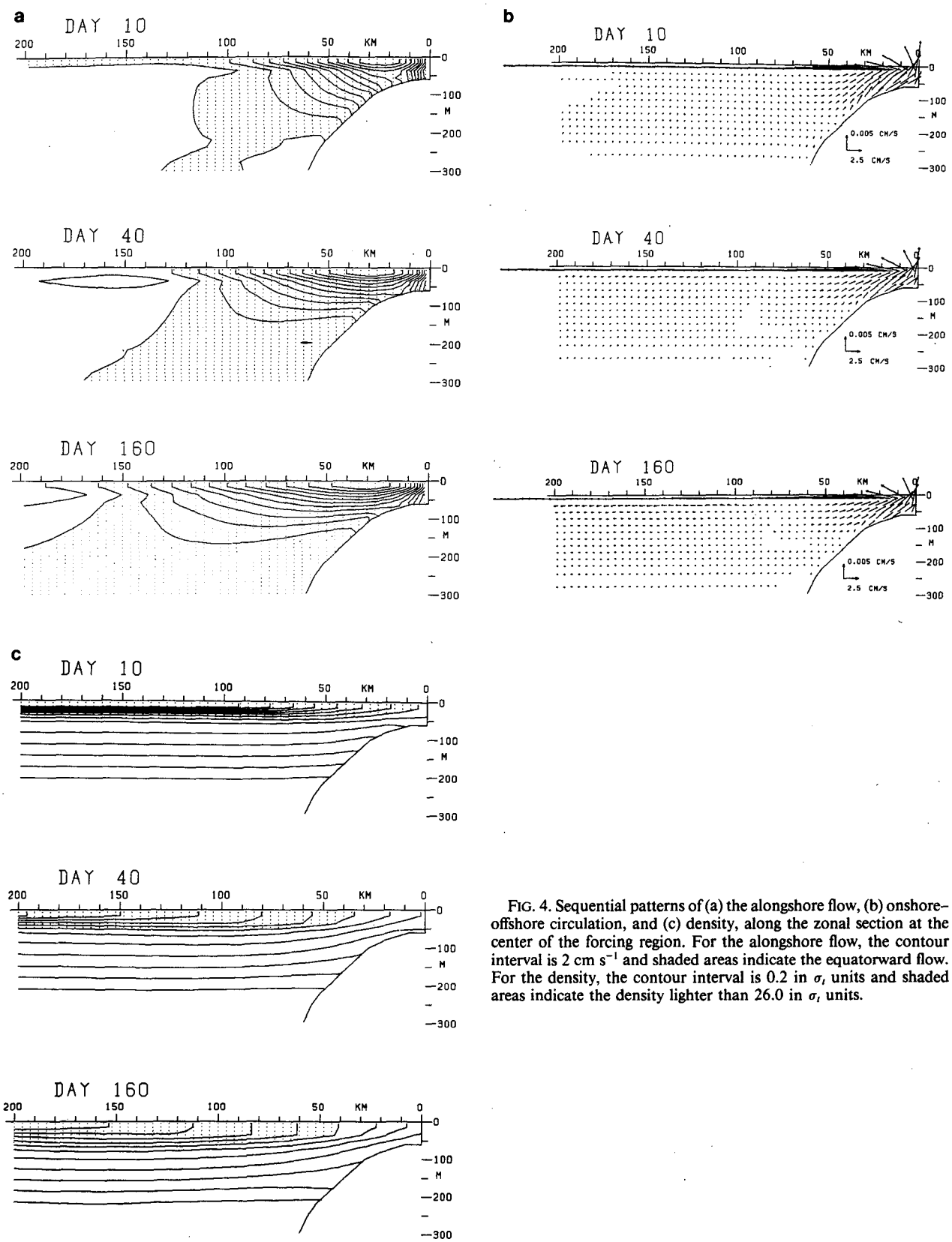

FIG. 4. Sequential patterns of (a) the alongshore flow, (b) onshore–offshore circulation, and (c) density, along the zonal section at the center of the forcing region. For the alongshore flow, the contour interval is 2 cm s^{-1} and shaded areas indicate the equatorward flow. For the density, the contour interval is 0.2 in σ_t units and shaded areas indicate the density lighter than 26.0 in σ_t units.

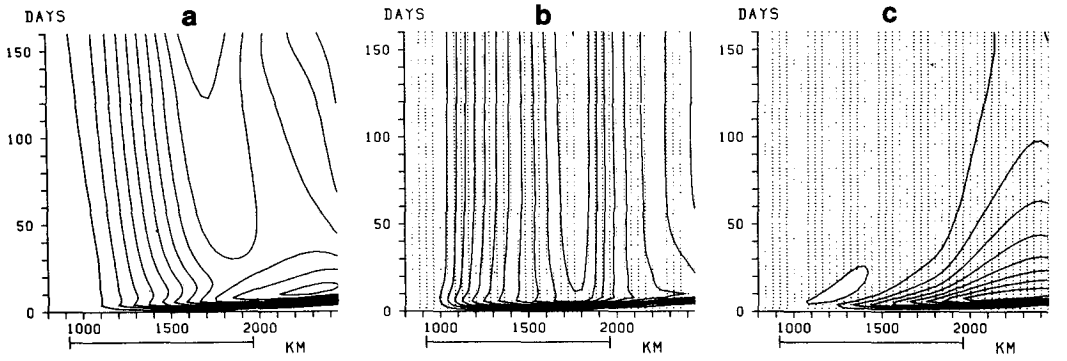

FIG. 5. Time evolution of the streamfunction (a) along the meridional line 112 km from the coast, alongshore flow (b) along the line 24 km from the coast at a depth of 10 m and (c) along the line 48 km from the coast at 170 m. The contour intervals are 2×10^{11} cm^3 s^{-1} for (a), 3 cm s^{-1} for (b) and 1.5 cm s^{-1} for (c). The forcing region is marked at the bottom of each figure.

undercurrent commences to develop. When the second-mode wave arrives, the poleward undercurrent and the coastal jet stop accelerating. The remaining modes keep evolving, and the undercurrent tends to weaken and finally disappears. After that, insignificant changes in upwelling circulation occcur. The higher mode waves are greatly affected by dissipation, and the solution gradually approaches its steady state. The passage of the mode waves leads to the three-dimensional upwelling circulation. In the forcing region, the coastal jet is stronger to the north, and the poleward undercurrent appears later and lasts longer in the northern region (Fig. 5b, c).

Only equatorward flow exists over the shelf–slope at the advanced stage. This is a fundamental difference from a flat bottom ocean studied by McCreary (1981) and Yoon and Philander (1982) in that an undercurrent is reproduced. Thus, the different mode structures yield significant differences in the upwelling circulation even at the advanced stage.

Effects of the bottom friction were examined for this f-plane model. The form and magnitude of the bottom friction coefficient are the same as in Semtner and Mintz (1977). Only minor modification is obtained. The poleward undercurrent tends to exist at slightly shallower depths, and it persists somewhat longer. However, the whole region over the shelf–slope has equatorward flow at the advanced stage.

b. The β-plane case

Next we discuss how β affects the long-term coastal upwelling. The Coriolis parameter is taken to be 5×10^{-5} s^{-1} at the center of the forcing region, and β is 2×10^{-13} cm^{-1} s^{-1}.

Sequential patterns of the alongshore flow and onshore–offshore circulation along the zonal section at the center of the forcing region are shown in Figs. 6a and b. The early-stage response within a week or so after the onset of the winds is similar to the f-plane case. However, a significant change in upwelling circulation takes place after the passage of the second-mode wave from the southern edge of the forcing region around day 17 (see also Fig. 9). The undercurrent below the thermocline tends to decrease in strength as in the f-plane case, but a shallower poleward undercurrent commences to develop in the thermocline layer over the shelf (see day 20 through day 40 in Fig. 6a). Then, this shallower undercurrent gradually increases in strength and spreads offshore. The flows in the surface layer also spread offshore with the core of the coastal jet remaining near the coast. It is worth noting that the remarkable offshore spreading of the surface equatorward flow obtained in Philander and Yoon (1982) for a flat bottom model is not developed here. For the onshore–offshore circulation, a significant difference from the f-plane case is the offshore spreading of the onshore flow in the surface layer.

The density field is similar to the f-plane case (see Fig. 4c). The coastward deepening of the isopycnals of the lower thermocline corresponds to the existence of the poleward undercurrent for the present β-plane model.

Horizontal distributions of the alongshore flow at depths 10, 90, 130 and 170 m at day 200 are shown in Fig. 7. The equatorward coastal jet is confined to the forcing region and the speed is less than for the f-plane case, especially in the northern area. The core of the poleward undercurrent exists over the shallower part of the shelf in the southern part of the forcing region and increases in depth to the north.

Next, we examine the sequential patterns of the streamfunction field, which may help determine what causes the difference between the f- and β-plane cases (Fig. 8). In the early-stage response, an anticyclonic vortex in the streamfunction field is formed in the forcing region and spreads poleward with the whole forcing region being occupied by the offshore transport (see day 10). From day 10 through day 40, a significant decrease of the equatorward transport takes place, predominantly in the northern area. Of course, this does not happen for the f-plane case. Then, the transport

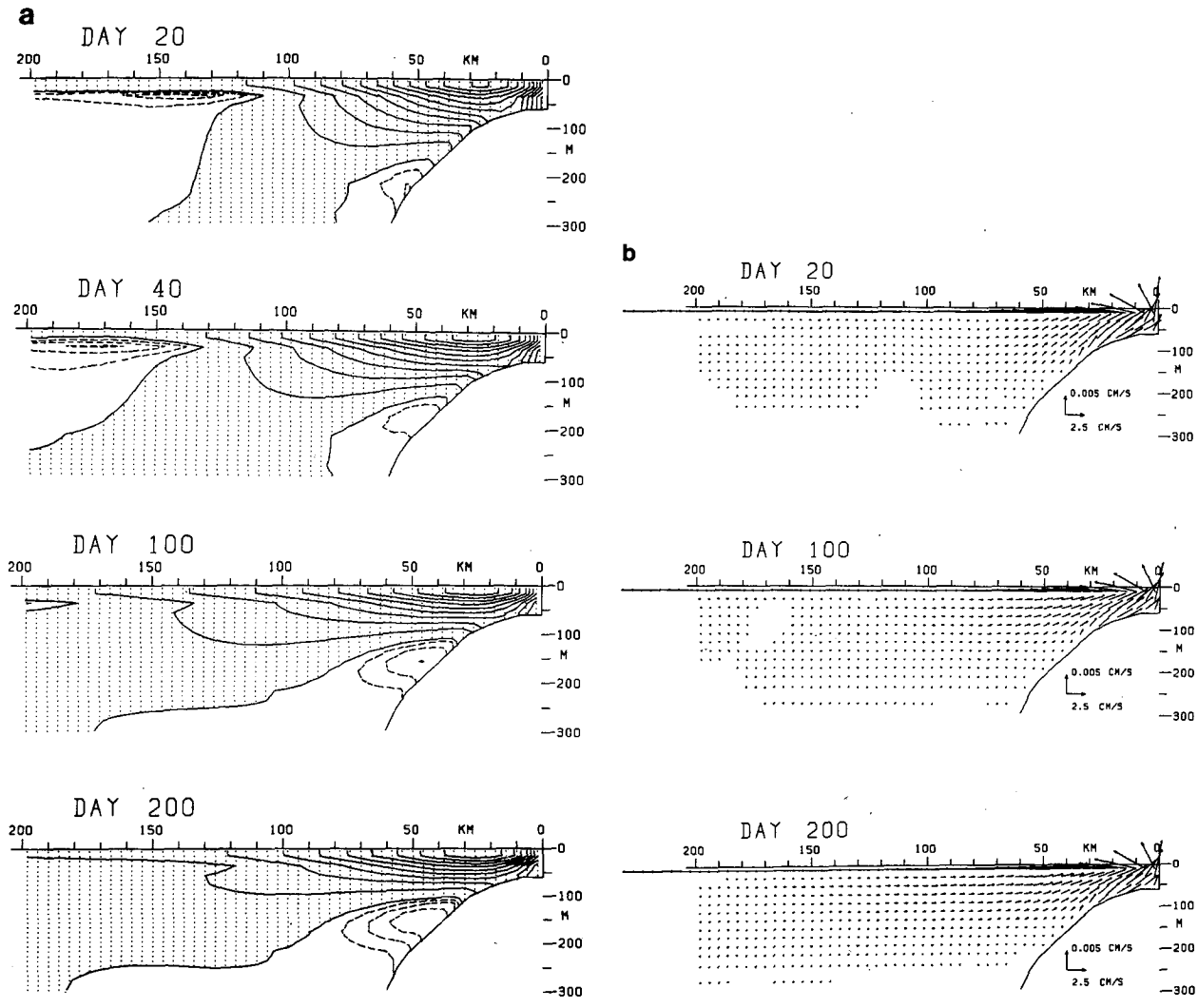

FIG. 6. As in Fig. 4 but for the β-plane case, (a) and (b) only. The dashed lines are at intervals of 0.5 cm s^{-1} for the poleward flow.

gradually decreases, eventually forming a weak anticyclonic vortex with its center in the northern part of the forcing region. This vortex is induced by the development of a frontal structure. At the advanced stage, the streamlines north of the forcing region are almost along contours of potential vorticity, f/H where H is the depth.

As in the f-plane case, the initial evolution of the upwelling circulation is accounted for by coastal-trapped wave dynamics. To see the differences between the f- and β-plane cases, first we discuss the time evolution along the coast. In Figs. 9a, b and c, the time evolution of the streamfunction and alongshore flow along the coast are plotted. The streamfunction field ceases to develop with the arrival of the first-mode wave. Then, the offshore transport in the forcing region tends to decrease in strength, though variations occur with the passage of the second-mode wave. A marked decrease in offshore transport evident in Fig. 8 is clearly observed in the northern part of the forcing region (compare Fig. 5a). For the alongshore flow, the formation of the coastal jet is almost completed with the arrival of the first-mode wave, and the jet approaches gradually to its steady state after the second-mode wave passes through. There is a marked decrease in speed in the northern area (compare Fig. 5b), and this decrease seems to be associated with the weakening of the transport. The poleward undercurrent at a depth of 170 m is first formed after passage of the first-mode wave; it tends to decrease in strength after the passage of the second-mode wave as seen in the southern part of the forcing region. However, for this β-plane model, the undercurrent recovers its strength and shows an additional development (compare Fig. 5c). This feature commences first near the southern edge of the forcing region, but it is not accounted for by coastal-trapped wave dynamics alone.

Next we discuss the β effect by examining the time

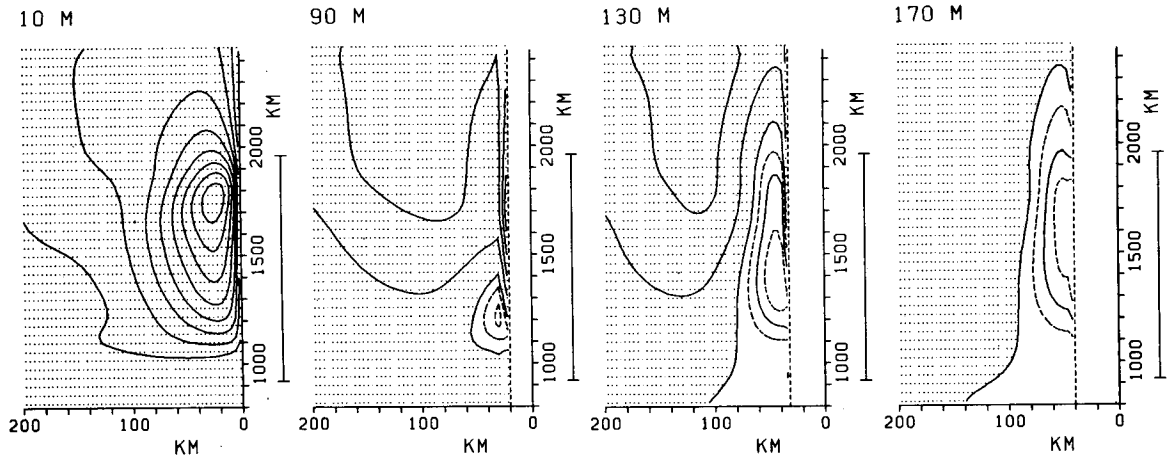

FIG. 7. Horizontal distributions of the alongshore flow at depths of 10, 90, 130 and 170 m at day 200. Contour intervals are 3 cm s^{-1} at 10 m and 1 cm s^{-1} at other depths. Dashed lines are at intervals of 0.5 cm s^{-1} for the poleward flow. Shaded areas indicate the equatorward flow. Forcing region is marked on the right side of each figure.

evolution along the zonal line at the center of the forcing region (Figs. 10a, b and c). With the arrival of the first-mode wave around day 5, the streamfunction field ceases to develop, yielding equatorward transport over the shelf–slope. Then westward dispersion of this equatorward transport takes place and persists for a long time. The two ridges and a trough in the pattern present in the offshore area are features associated with the passage of the second-mode wave around day 17. This wave is strongly affected by westward Rossby dispersion and so extends well offshore. As seen in the patterns in the offshore area, the speed of the dispersion is larger at early rather than at advanced stages. Development of the equatorward flow over the shelf–slope is also completed with the arrival of the first-mode wave, and then the equatorward flow at deeper depths significantly decreases in strength. The reason is that the equatorward flow at all depths tends to spread westward. This dispersion is not significant in the surface layer but it is at deeper depths. The dispersion is particularly evident as a ridge in the pattern over the shelf–slope at the depth of 130 m where the core of the undercurrent exists along this section. It seems that the undercurrent tends to develop in association with this westward dispersion which commences after the passage of the second-mode wave around day 17. In the flat bottom area, as apparent in the patterns of the streamfunction and alongshore flow, the dispersion is neither purely barotropic nor baroclinic.

Along zonal lines at other latitudes, a similar westward Rossby dispersion takes place. The westward dispersion of the equatorward transport within about 40 days is predominant at high latitudes as seen in Fig. 8. For the alongshore flow, the speed of dispersion over the shelf–slope is larger at low than at high latitudes, though the difference in speed is small. This dispersion commences after the passage of the second-mode wave,

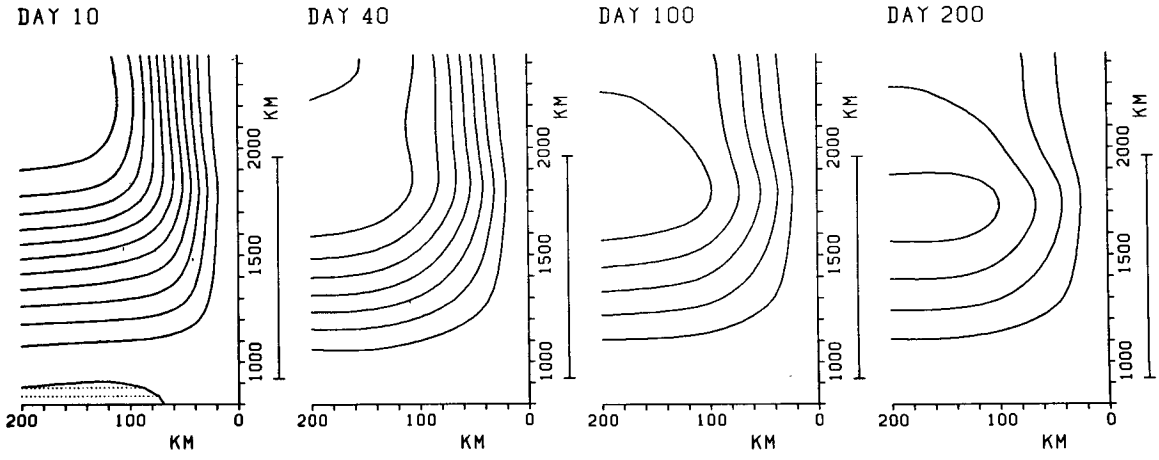

FIG. 8. Sequential patterns of the streamfunction field. The contour intervals are 2×10^{11} cm^3 s^{-1}.

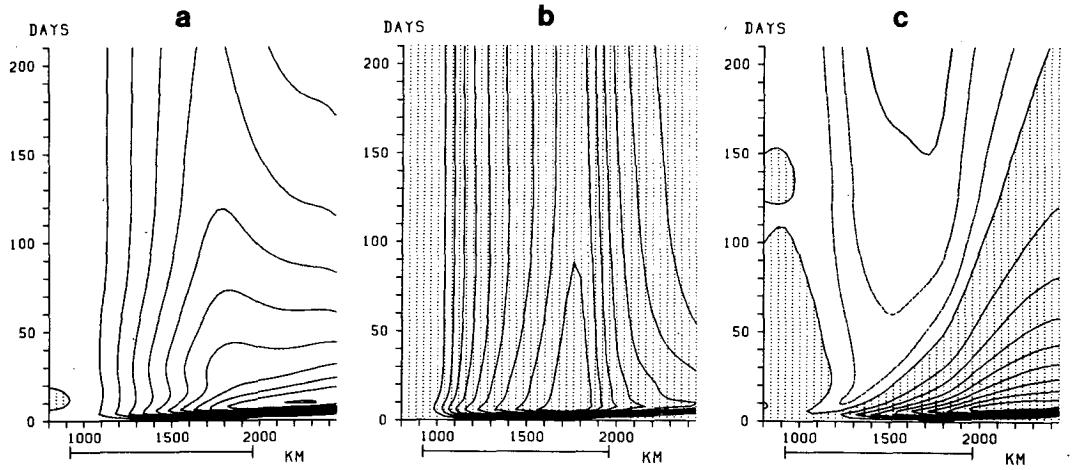

FIG. 9. As in Fig. 5 but for the β-plane case. The dashed lines are at intervals of 0.5 cm s^{-1} for the poleward flow.

and the appearance of the undercurrent is more advanced in low than high latitudes (Fig. 9). North of the forcing region, the dispersion of the surface equatorward flow is more remarkable, leading to the concentration of the coastal jet inside the forcing region as seen in Fig. 7.

As studied in McCreary (1981) and Philander and Yoon (1982) for a flat bottom ocean, a marked Rossby dispersion takes place for the lower vertical modes. For the present model with a continental shelf–slope, the marked westward dispersion of the equatorward transport over the shelf–slope occurs early, within about 40 days, predominantly in the northern area. Also the gradual dispersion of the equatorward transport, which involves the subsurface equatorward flow, persists for a long time. These features, with the difference of the alongshore flow patterns over the shelf–slope between the f- and β-plane cases, indicate that the dispersion found at the early stage is that for the first-mode response, and the gradual dispersion is that for the second-mode response.

We also calculated a case where the Coriolis parameter at the center of the forcing area is twice that in the previous case, i.e., $f = 10^{-4}$ s^{-1}. Since propagation speeds of the coastal-trapped waves become larger as studied in I, the increase in the Coriolis parameter leads to speedup of the early-stage evolution of the upwelling circulation. Of course, the speedup of evolution yields a decrease in amplitude of the lower mode responses. The initial westward dispersion of the equatorward transport takes place in a similar way to that of the previous lower latitude case. However, the dis-

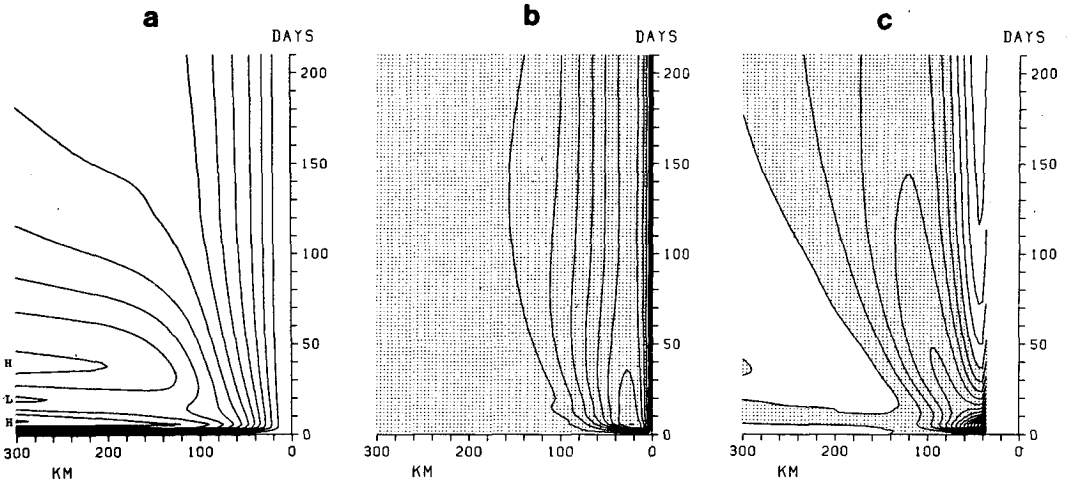

FIG. 10. Time evolution of the streamfunction and alongshore flow along the zonal line at the center of the forcing region: (a) streamfunction (contour interval is 10^{11} cm^3 s^{-1}); (b) alongshore flow at a depth of 10 m (contour interval is 3 cm s^{-1}); (c) alongshore flow at a depth of 130 m (contour interval is 0.5 cm s^{-1}). For alongshore flow, shaded areas indicate the equatorward flow.

persion of the second-mode response is significantly slowed, and appearance of the poleward undercurrent in the thermocline layer is delayed significantly, by almost a hundred days. Thus, it may be concluded that the dispersion of the second-mode response determines the occurrence of the poleward undercurrent.

4. Discussion and conclusion

The long-term coastal upwelling over a shelf–slope with emphasis on the planetary dispersion of Rossby waves has been studied with numerical models. The ocean is forced by wind stress with a limited longshore extent. The thermocline intersects the shelf–slope and the internal radius of deformation is smaller than the width of the shelf–slope. This is a typical situation for the coastal upwelling regions, such as those off California and Oregon. Two case studies, with and without the β effect, have been considered.

The early-stage response within a week or so is similar between the two cases; it has been discussed in detail in I. It is re-emphasized that the coastal-trapped waves, which can be identified neither as barotropic shelf nor as internal Kelvin waves, play a fundamental role in determining the upwelling circulation. For the f-plane case, the whole-stage response is accounted for by coastal-trapped wave dynamics, and only equatorward flow exists over the shelf–slope at the advanced stage. However, inclusion of the β effect leads to a significant change in the alongshore flow pattern at the advanced stage. Due to the westward Rossby wave dispersion of the equatorward flow associated with the first and second mode responses, the poleward undercurrent develops in the thermocline layer. The core of the undercurrent exists over the shallower part of the shelf in the southern part of the forcing region and increases in depth to the north. The time for the undercurrent to appear depends on the speed of the westward dispersion of the second-mode response. With decreasing latitude, the appearance speeds up.

Westward Rossby dispersion is different between cases with and without a continental shelf–slope. In a flat bottom model of Philander and Yoon (1981), the remarkable offshore spreading of the equatorward surface flow takes place. This is because the surface flow which disperses westward consists of the lower, internal Kelvin mode responses, and the lower modes have larger speeds for the westward propagation. The dispersion is more advanced at low rather than high latitudes, since internal Rossby waves propagate more rapidly at low latitudes. However, in the present model with a shelf–slope, although the westward dispersion of the lower mode responses takes place, the remarkable offshore spreading of the surface flow is not developed. This is due to the different coastal response structures which are determined by the coastal-trapped wave modes (structures of the alongshore flow for the first and second coastal-trapped modes are illustrated in I).

Dispersion of the first-mode response commences after the passage of the first-mode wave; it seems to take place along contours of potential vorticity, f/H. In the area where the contours originating from the forcing region connect to the flat bottom area, this dispersion is significant. Dispersion of the second-mode response commences after the passage of the second-mode wave, and the speed is larger at low than high latitudes. The dispersion speed for the second mode may be associated with that of internal Rossby waves offshore, but further details of the dispersion have not been clarified in the present study. Moreover, in the flat-bottom offshore area, the barotropic and baroclinic Rossby modes exist, instead of complicated vertical structure associated with the coastal-trapped modes in the coastal area. The energy conversion from coastal-trapped modes to barotropic and baroclinic modes has also not been clarified here. Coastal-trapped waves in the presence of the β effect need further study.

In the present study for the β-plane case, the calculation is stopped at day 210. The gradual westward dispersion remains even for the poleward undercurrent. For a flat-bottom ocean, as McCreary (1981) and Philander and Yoon (1982) pointed out, dissipation is essential for obtaining nonzero, steady-stage alongshore flow such as the coastal jet and the poleward undercurrent along eastern boundary. For the present model with a shelf–slope, if the fluid is inviscid, no alongshore flow may remain in the deeper ocean in the wake of the Rossby dispersion. This may be speculated from the results for an inviscid linear two-layer general circulation model with bottom topography (Miura and Suginohara, 1980; Anderson and Killworth, 1977), because there is no direct forcing in the lower layer. Therefore, it may be stated that even for the present model, dissipation is essential for obtaining a poleward undercurrent at a steady state and that our solution is not far from a steady state.

Direct current measurements off Oregon show that the poleward undercurrent over the shelf exists as a mean alongshore flow only in late summer (Huyer *et al.*, 1975). This phenomenon may be reproduced in the present β-plane model in that at high latitudes the appearance of the undercurrent is delayed significantly. Off California, recent observations show that the undercurrent exists at mid-depth over the midshelf and persists at least from spring through summer (Allen, personal communication, 1983). Thus, the poleward undercurrent over the shelf obtained in the present model may represent the observed poleward undercurrent, although the magnitude is not adequately reproduced. In other words, the observed undercurrent over the shelf may be the flow associated with coastal upwelling induced by regional winds with a large time scale. Along the west coast of the United States, a rather strong poleward undercurrent exists over the slope, the California Undercurrent (Hickey, 1979). It seems to the authors that the California Undercurrent

may not be induced by regional winds, but it may be related to the more global tropical circulation which is affected by the presence of the continental shelf–slope (Kitamura and Suginohara, personal communication, 1983).

Acknowledgments. The authors thank Drs. K. Kajiura and J.-H. Yoon for pleasant discussions. Their thanks are extended to Drs. J. P. McCreary and C. N. K. Mooers for reading the manuscript and making very helpful comments. Thanks also to Ms. T. Osada for drafting the figures and typing the manuscript.

REFERENCES

Anderson, D. L. T., and P. D. Killworth, 1977: Spin-up of a stratified ocean, with topography. *Deep-Sea Res.*, **24,** 709–732.

Hickey, B. M., 1979: The California Current System—hypotheses and facts. *Progress in Oceanography,* Vol. 8, Pergamon, 191–279.

Huthnance, J. N., 1978: On coastal trapped waves: Analysis and numerical calculation by inverse iteration. *J. Phys. Oceanogr.*, **8,** 74–92.

Huyer, A., 1976: A comparison of upwelling events in two locations: Oregon and northwest Africa. *J. Mar. Res.*, **34,** 531–546.

——, R. D. Pillsbury and R. L. Smith, 1975: Seasonal variation of the alongshore velocity field over the continental shelf off Oregon. *Limnol. Oceanogr.*, **20,** 90–95.

McCreary, J. P., 1981: A linear stratified ocean model of the Coastal Undercurrent. *Phil. Trans. Roy. Soc. London,* **A302,** 385–415.

Miura, H., and N. Suginohara, 1980: Effects of bottom topography and density stratification on the formation of western boundary currents, Part I: Wind driven general circulation model. *J. Oceanogr. Soc. Japan,* **35,** 215–223.

Philander, S. G. H., and J.-H. Yoon, 1982: Eastern boundary currents and coastal upwelling. *J. Phys. Oceanogr.*, **12,** 862–879.

Semtner, A. J., and Y. Mintz, 1977: Numerical simulation of the Gulf Stream and mid-ocean eddies. *J. Phys. Oceanogr.*, **7,** 208–230.

Suginohara, N., 1977: Upwelling front and two-cell circulation. *J. Oceanogr. Soc. Japan,* **33,** 115–130.

——, 1982: Coastal upwelling: Onshore–offshore circulation, equatorward coastal jet and poleward undercurrent over a continental shelf–slope. *J. Phys. Oceanogr.*, **12,** 272–284.

Yoon, J.-H., and S. G. Philander, 1982: Formation of the coastal undercurrents. *J. Oceanogr. Soc. Japan,* **38,** 215–224.